



HAL
open science

Non-linear inversion modeling for Ultrasound Computer Tomography: transition from soft to hard tissues imaging

Philippe Lasaygues, Serge Mensah, Régine Guillermin, Julien Rouyer, Emilie Franceschini

► To cite this version:

Philippe Lasaygues, Serge Mensah, Régine Guillermin, Julien Rouyer, Emilie Franceschini. Non-linear inversion modeling for Ultrasound Computer Tomography: transition from soft to hard tissues imaging. Non-linear inversion modeling for Ultrasound Computer Tomography: transition from soft to hard tissues imaging, Feb 2012, San Diego, United States. pp.1-14. hal-00721371

HAL Id: hal-00721371

<https://hal.science/hal-00721371>

Submitted on 27 Jul 2012

HAL is a multi-disciplinary open access archive for the deposit and dissemination of scientific research documents, whether they are published or not. The documents may come from teaching and research institutions in France or abroad, or from public or private research centers.

L'archive ouverte pluridisciplinaire **HAL**, est destinée au dépôt et à la diffusion de documents scientifiques de niveau recherche, publiés ou non, émanant des établissements d'enseignement et de recherche français ou étrangers, des laboratoires publics ou privés.

Non-linear inversion modeling for Ultrasound Computer Tomography: transition from soft to hard tissues imaging

Philippe Lasaygues, Serge Mensah, Régine Guillermin, Julien Rouyer, Emilie Franceschini

Laboratory of Mechanics and Acoustics, UPR CNRS 7051, Aix-Marseille University, Centrale Marseille, F-13402
Marseille cedex 20, France

ABSTRACT

Ultrasound Computer Tomography (UCT) is an imaging technique which has proved effective for soft-tissue (breast, liver,...) characterization. More recently, the use of UCT has been envisaged for bone imaging. In this field, the large variations of impedance distribution (high contrast) require that a finer model of wave propagation be integrated into the reconstruction scheme. Here, the tomographic procedure used is adapted to broadband data acquired in scattering configurations while the heterogeneous objects (Born approximation) are probed by spherical waves. An “elliptical” Fourier transform has been derived to solve the near-field inverse problem. This transform differs from the standard Fourier Transform in that, instead of plane waves, families of harmonic ellipsoidal waves are considered. For soft tissues it is possible to separate the impedance and speed of sound contributions and to reconstruct their cartographies using dedicated near-field Radon transforms. In the case of highly heterogeneous media such as bones, iterative inversion schemes are proposed. The various reconstruction procedures are set against experiments.

Keyword: Ultrasound Computer Tomography, Inverse Born Approximation, Elliptical Projection, Iterative Approximation, Soft Tissues Imaging, Hard Tissues Imaging, Breast, Bones

1. INTRODUCTION

This paper presents the theoretical framework that enables one, with a unified formulation, to find specific responses, on the one hand, to the problem of soft tissue imaging (dedicated to breast cancer detection) and, on the other hand, to the problem of bone characterization (dedicated to osteoporosis, bone infection and cancer). The difficulties raised are somewhat different as, in soft tissues, the very small fluctuations to be quantified suffer from their very low values. This poor echogenic index generally induces low detection probability, for instance in the case of large diffuse masses. In addition, invasive lesions that must not be overlooked may be of millimetric size. In bone imaging, the difficulties arise from the very high contrast that strongly alters the propagation of the ultrasonic waves. Solutions consist in optimally assessing these non-linear effects in an iterative approach aiming at local linearization.

In this article we describe a near field UCT method based on the use of the first-order Born approximation, applied to the case of an homogeneous and constant background. The unknown object function, which is assumed to be weakly heterogeneous, is linearly related to the field measured via a tool called the Elliptical Fourier transform. The inverse problem is related to an extension of the filtered back-projection algorithm. This technique is suitable for breast inspection where the probe is either in contact with the skin or located within a near field distance when using a coupling device (water bag or water tank).

However the first-order Born UCT has some limitations when dealing with highly contrasted scatterers. When the problem can be reduced to the study of a fluid-like cavity buried in an elastic cylinder surrounded by water, we have proposed an extension of this method, by taking into account physical phenomena such as wave refraction [1, 2, 3, 4]. The approach, named Compound Quantitative Ultrasonic Tomography - CQUT, is purely experimental and consists in performing reflection and transmission measurements, using an iterative correction procedure, which compensates for refraction effect arising at the boundary between bone and the surrounding tissues. The main limitation of the CQUT method is the heavy experimental-costs involved (multiple iterative experiments), and we suggest a purely numerical non-linear inversion algorithm, named the Distorted Born Diffraction Tomography – DBDT, in which the application of

the Born approximation is extended to higher orders [5]. In comparison with the previous upgrade, DBDT combines diffraction measurements [6].

The performances and limitations of these tomographic methods applied to breast and bone imaging problems are presented.

2. FORMULATION

2.1. Soft-tissue forward problem

Ultrasound Computer Tomography (UCT) applied to soft tissues, (we confine ourselves to breast inspection), has been studied in several scientific research projects [7, 8] and the use of powerful computers makes it possible nowadays to introduce rather complex algorithms [9,10]. Numerous experimental devices have also been developed [11,12,13]. In these approaches, breast tissues are described by means of acoustical models, the mechanical parameter pairs can be either (density, compressibility) or (density, speed of sound); we adopt an (impedance, speed of sound) formulation since these parameters offer separate contributions in transmission and in reflection. Let ρ_0, c_0 be the acoustic characteristics of the homogeneous coupling medium, and let us introduce the contrast parameter functions of speed of sound and of the acoustical impedance:

$$\alpha(\underline{x}) = \frac{c^2(\underline{x}) - c_0^2}{2c^2(\underline{x})} \quad \text{and} \quad \xi(\underline{x}) = \text{Log}\left(\frac{z}{z_0}\right), \quad (1)$$

the governing pressure propagation equation is written:

$$-\frac{1}{c_0^2} \frac{\partial^2 p}{\partial t^2} + \nabla^2 p \equiv S \equiv -\frac{2\alpha}{c_0^2} \frac{\partial^2 p}{\partial t^2} - \nabla \alpha \nabla p + \nabla \xi \nabla p. \quad (2)$$

The object to be inspected is excited with a spherical wave having an infinite frequency band:

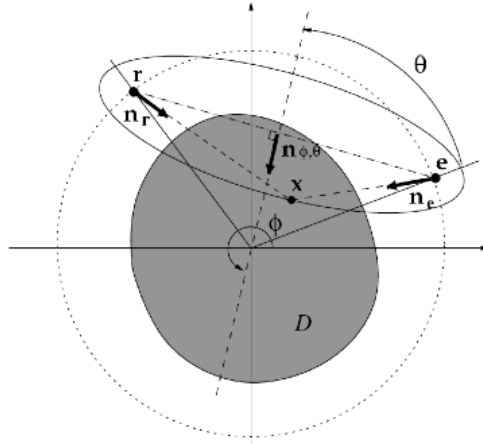


Figure 1: Scattering acquisition configuration in acoustic tomography: the punctual source located in e corresponds to the focus of the spherical transmitter, the receiver focus is in r.

$$P_i(\underline{x}, \underline{e}, t) = \delta\left(t - \frac{|\underline{x} - \underline{e}|}{c_0}\right) \frac{1}{4\pi|\underline{x} - \underline{e}|} \quad (3)$$

Let us consider the differential distribution:

$$v_e(\underline{x}, t) = -\underline{n}_e \left(\frac{1}{|\underline{x} - \underline{e}|} \delta(t) - \frac{1}{c_0} \delta'(t) \right) \quad (4)$$

unit vector \underline{n}_e is shown on Figure 1, the prime stands for the first derivation and let us note:

$$\begin{aligned} S(\underline{x}, \underline{e}, t) &= S^*(\underline{x}, \underline{e}, t) *_i p_i(\underline{x}, \underline{e}, t) \\ &= \left[-\frac{2\alpha}{c_0^2} \delta''(t) - [\nabla \alpha - \nabla \xi] v_e \right] *_i p_i(\underline{x}, \underline{e}, t), \end{aligned} \quad (5)$$

The temporal support of $S^*(\underline{x}, \underline{e}, t)$ being of null width (sum of derivatives of Dirac's distribution), in case of spherical transmitted waves (small pitch transducer), one can easily derive the integral expression of the scattered field :

$$\begin{aligned} p_d(\underline{r}, \underline{e}, t) &= - \int_{\mathbb{R}^3} \frac{\delta \left(t - \frac{|r - \underline{x}|}{c_0} - \frac{|\underline{x} - \underline{e}|}{c_0} \right)}{16\pi^2 |r - \underline{x}| |\underline{x} - \underline{e}|} *_i S^*(\underline{x}, \underline{e}, t) d\underline{x} \\ &= - \int_{\Sigma_t} \frac{S^* \left(\underline{x}, \underline{e}, t - \frac{|r - \underline{x}|}{c_0} - \frac{|\underline{x} - \underline{e}|}{c_0} \right)}{16\pi^2 |r - \underline{x}| |\underline{x} - \underline{e}|} d\underline{x}. \end{aligned} \quad (6)$$

Ellipse Σ_t of foci $(\underline{x}, \underline{r})$ is defined by the relation $c_0 t = |r - \underline{x}| + |\underline{x} - \underline{e}|$. Then, $p_d(\underline{x}, \underline{e}, t)$ is the elliptical projection onto Σ_t of the source terms. Given the two points \underline{e} and \underline{r} , the former expression can be rewritten in its integral form marked by « $\widehat{*}$ »:

$$\begin{aligned} G \widehat{*} S(\underline{r}, \underline{e}, t) &= \int_{\mathbb{R}^3} \frac{\delta \left(t - t' - \frac{|r - \underline{x}'|}{c_0} \right)}{4\pi |r - \underline{x}'|} S(\underline{x}', \underline{e}, t') d\underline{x}' dt' \\ &= \int_{\mathbb{R}^3} \frac{\delta \left(t - t' - \frac{|r - \underline{x}'|}{c_0} \right)}{4\pi |r - \underline{x}'|} S^* *_i p_i(\underline{x}', \underline{e}, t') d\underline{x}' dt' \end{aligned} \quad (7)$$

Hence the synthetic expression of the scattered field (Born approximation) :

$$p_d(\underline{r}, \underline{e}, t) = G \widehat{*} S(\underline{r}, \underline{e}, t) = G \widehat{*} S^* *_i p_i(\underline{r}, \underline{e}, t) \quad (8)$$

If instead of a spherical wave of infinite bandwidth one uses a harmonic spherical transmit wave, then (7) becomes:

$$\begin{cases} p_d(\underline{r}, \underline{e}, \omega) = - \int_{\Sigma_t} \frac{e^{ik(|r - \underline{x}| + |\underline{x} - \underline{e}|)}}{16\pi^2 |r - \underline{x}| |\underline{x} - \underline{e}|} S^*(\underline{x}, \underline{e}, \omega) d\underline{x} \\ \hat{v}_e(\underline{x}, \underline{e}, \omega) = \underline{n} \left(\frac{1}{|\underline{x} - \underline{e}|} - ik \right) \\ S^*(\underline{x}, \underline{e}, \omega) = k^2 2\alpha - [\nabla \alpha - \nabla \xi] \hat{v}_e(\underline{x}, \underline{e}, \omega) \end{cases} \quad (9)$$

The first of these expressions reveals a transform similar in its form to the standard Fourier transform. It is specified by the harmonic decomposition functions having as spatial support a time-indexed ellipsoid, and for foci the loci of the

transmitter and of the receiver. This decomposition has been named the Elliptical Fourier transform (EFT). We have shown in a previous paper [14] that this transform is invertible. Thus, the scattered field is the ellipsoidal spectrum of the secondary source term specified by the acoustical parameters.

Nota 1: In the harmonic regime, since the harmonic functions are the eigen functions of the temporal convolution operator, (8) is written:

$$p_d(\underline{r}, \underline{e}, \omega) = G \hat{*} S(\underline{r}, \underline{e}, \omega) = \left[G \hat{*} (S^* \times p_i) \right](\underline{r}, \underline{e}, \omega) \quad (10)$$

Nota 2: When no confusion is possible, for any well-behaved function f , $f(\underline{r}, \underline{e}, \omega)$ refers to the spectrum of function $f(\underline{r}, \underline{e}, t)$. When distinction is required the spectrum is also noted: $f(\underline{r}, \underline{e}, \omega) = \hat{f}(\underline{r}, \underline{e}, \omega) = \hat{f} = F[f(\underline{r}, \underline{e}, t)]$, F is the standard Fourier transform.

Nota 3: When source term S^* corresponds to a harmonic plane wave, excitation can be easily detailed from (9). Indeed, in that case, the source locus \underline{e} is “pushed away” to infinity and $\hat{v}_e(\underline{x}, \underline{e}, \omega) = -\underline{n}_0 ik$ (\underline{n}_0 is the unit vector in the incident direction). Thus,

$$S^*(\underline{x}, \omega) = k^2 2\alpha(\underline{x}, \omega) - ik\underline{n}_0 [\nabla\alpha(\underline{x}, \omega) - \nabla\xi(\underline{x}, \omega)] \quad (11)$$

This is the result obtained in ultrasound tomography development using far-field measurements and standard Back-Projection (BP) algorithm [11]. We observe here the possibility of continuously adjusting the inversion operator from far field down to near field thanks to $\hat{v}_e(\underline{x}, \underline{e}, \omega)$ vector.

Then, applying the EFT (overlined with an arrow) to the formulations in (8) and considering the specific derivation rules related to the elliptical analysis [14], one obtains:

$$\begin{cases} \hat{\underline{v}}(\underline{x}, \omega) = \hat{\underline{v}}_e(\underline{x}, \omega) - \hat{\underline{v}}_r(\underline{x}, \omega) \\ \underline{K} = k\underline{n}_{\varphi, \theta} \\ -p_d(\underline{K}) = k^2 2\bar{\alpha}(\underline{K}) - (\hat{\underline{v}}_e \cdot \hat{\underline{v}}) * [\bar{\alpha} - \bar{\xi}](\underline{K}) \end{cases} \quad (12)$$

The scattered field is the result of the convolution in the elliptical spectral domain of the elliptical spectra with the directivity index functions. If the transmitter (resp. receiver) /pixel distances are of the order of the wavelength, we obtain with a good approximation

$$\hat{\underline{v}}_e \cdot \hat{\underline{v}} \approx -k^2 (1 + \underline{n}_e \cdot \underline{n}_r), \text{ where } \underline{n}_l = \nabla(|\underline{x} - \underline{l}|) \quad (13)$$

\underline{n}_e is the unit vector in the direction transmitter (resp. receiver) / voxel. Then, the system is reduced to:

$$p_d(\underline{K}) = -k^2 \left[(\overline{1 - \underline{n}_e \cdot \underline{n}_r}) * \bar{\alpha} - (\overline{1 + \underline{n}_e \cdot \underline{n}_r}) * \bar{\xi} \right](\underline{K}) \quad (14)$$

Indeed, these equations involve two acoustical parameters offering distinct directivity patterns that can be separated according to the spatial scanning performed:

- $\underline{n}_e = -\underline{n}_r$, $p_d = k^2 \bar{\alpha}$, in pure transmission, the scattered field is conditioned by the quadratic fluctuations of the sound speed.
- $\underline{n}_e = \underline{n}_r$, $p_d = k^2 \bar{\xi}$, in pure reflection, the scattered field results from impedance fluctuations.

These results are coherent with those obtained using plane wave excitation and plane wave decomposition (standard Fourier transform). Here, they are extended in the sense that the analysis has been done taking into account the curvature of the “elliptical” wavefront.

2.2. “Near-field” tomography

By applying the inverse elliptical Fourier transform to the elliptical spectra, it is possible to reconstruct the impedance or the sound speed maps since they are respectively obtained from pure reflection and transmission measurements.

1.1.1. Fast inversion procedure

For this purpose, the acquisition procedure consists in filling in the respective elliptical Fourier domains with the highest sampling densities by performing both a spatial scan and a frequency sweep using broadband signals. In practice, however, the transducers have a finite bandwidth and one may be able to reconstruct only a bandpass (respectively, low-

pass) filtered version of the impedance (respectively sound speed). Besides, rather than using multidimensional inverse elliptical Fourier transforms to retrieve the object from diffraction measures, it is better to use a reconstruction procedure based on classical one-dimensional (1D) Fourier transforms that are numerically optimised. Therefore, we have defined a near-field extension of the Radon transform and introduced an elliptical backprojection algorithm similar in its form to the standard backprojection (FBP) algorithm.

Let $f(\underline{x})$ be a well-behaved object function defined over the compact domain D of \mathbb{R}^2 . f represents one of the separable parameters specified above. For a given configuration angle $\theta = \theta_0$, (cf. Figure 1), we define the elliptical Radon transform for any pair $(s, \phi) \in \{s \in \mathbb{R}, 0 \leq \phi \leq \pi\}$ by:

$$[R_\epsilon f](s, \phi) = \int f(\underline{x}) \frac{\delta(s - |r - \underline{x}| - |\underline{x} - \underline{e}|)}{16\pi^2 |r - \underline{x}| |\underline{x} - \underline{e}|} d\underline{x} \quad , \quad (15)$$

and consider the projection $p_\phi(s)$ under incidence ϕ :

$$[R_\epsilon f](s, \phi)_{\phi, \text{fixed}} = p_\phi(s) \quad (16)$$

We introduce the scalar product:

$$\underline{n}_{\phi, \theta} \bullet \underline{x} = -(|r - \underline{x}| + |\underline{x} - \underline{e}|) \quad . \quad (17)$$

Here, its negative value results from the fact that the wave is propagating toward the origin, and is opposed to the outgoing orientation of axis \underline{x} .

We derive the synthesis of function f from its ellipsoidal decomposition (projections $p_\phi(s)$ under incidence ϕ):

$$f(\underline{x}) = \frac{1}{(2\pi)^2} \int_0^{\tilde{\pi}} \int_{-\infty}^{\infty} \hat{p}_\phi(S) |S| e^{iS \bullet \underline{x}} [\underline{x}]_\phi dS d\phi \quad (18)$$

This relation resembles the continuous expression of the classical backprojection algorithm. Except the normalization term, $[\underline{x}]_\phi = 16\pi^2 |r - \underline{x}| |\underline{x} - \underline{e}|$, accounting for the divergence of the beam, one can retrieve all the constitutive elements.

A difference however, which is worth noticing: the nature of the projection differs since, here, we consider an elliptical projection $p_\phi(s)$ over Σ_ϕ defined by:

$$s = c_0 t = \underline{S}_\phi \bullet \underline{x} = |r - \underline{x}| + |\underline{x} - \underline{e}| \quad , \quad (19)$$

1.1.2. Elliptical Backprojection (EBP) operator

Let us consider an arbitrary function $h(s, \phi)$ where $s = \underline{n}_\phi \bullet \underline{x}$, the elliptical backprojection operator is:

$$B[h(s, \phi)](\underline{x}) = \frac{1}{2} \times \frac{1}{\pi} \int_0^\pi [\underline{x}]_\phi h(\underline{n}_\phi \bullet \underline{x}, \phi) d\phi. \quad (20)$$

Function f is then recovered by EBP [12]:

$$f = B \circ F^{-1} \circ Abs \circ F \circ R_\epsilon \circ f = R_\epsilon^{-1} \circ R_\epsilon \circ f \quad (21)$$

where the response of filter Abs is $Abs(S) = |S|$.

Let us call p_{dm} the ‘‘measured scattered field’’ and S_{est}^* the estimated parameter map reconstructed from the data acquired; remember that S_{est}^* is bound either to the impedance map or to the speed of sound according to the protocol of acquisition (pure reflection or transmission). Under such conditions,

$$S_{est}^* = R_\epsilon^{-1} [p_{dm}] \quad (22)$$

Thus, the Elliptical Backpropagation Algorithm leads to an Inverse Born Approximation (IBA) with a (almost) ‘‘constant background’’ (considering the matching of the mean acoustical impedances).

1.1.3. "Hard-tissue" tomography

Modified elliptical Radon transform: With hard biological tissues having larger acoustical impedances and speed of sound than those of the surrounding medium, the weak scattering assumption is no longer realistic. Indeed, the transmitted wave is "deviated" from its initial course because of refraction. This results in a new distribution of the energy initially transmitted to the Region Of Interest (ROI). Consequently, only a small percentage of the incident energy penetrates into the contrasted medium, and the recorded signal is highly attenuated, especially as far as the high frequencies are concerned. Thus, if it is not taken into consideration prior to the inversion, this redistribution may lead to a loss of information; for instance, strong geometrical distortions or large shadows may occur. On the contrary, appropriate scanning of the highly contrasted medium can provide good qualitative imaging. In addition, if prior information is available, quantitative recovery of the parameter distributions may be expected.

Thus, due to the important sound speed and impedance fluctuations, the assumption that sound speed is constant in relations (7) and (8) is no longer valid. Instead, one has to take into account the spatial dependence of the speed of sound in the derivation of the scattered field:

$$p_d(r, \underline{e}, t) = - \int_{\Sigma_r} \frac{S^* \left(\underline{x}, \underline{e}, t + \tau(\underline{x}) - \frac{|r - \underline{x}|}{c_0} - \frac{|\underline{x} - \underline{e}|}{c_0} \right)}{16 \pi^2 |r - \underline{x}| |\underline{x} - \underline{e}|} d\underline{x} \quad (23)$$

Here, the temporal correction is approximated on the basis of straight line propagation inside the hard medium:

$$\tau(r, \underline{e}, \underline{x}) = \frac{1}{c_0} \int_{\underline{e} + \underline{x}r} \frac{c(\underline{x}') - c_0}{c_0} d\underline{x}' = \tau_e(\underline{x}) + \tau_r(\underline{x}) \quad (24)$$

Hence, the overall correction is the sum of the respective temporal corrections along the emitter-voxel (located in \underline{x}) path and along the voxel-receiver path.

Indeed, this correction term is unknown since the sound speed parameter is directly or indirectly sought for; it is generally estimated via an iterative tomographic procedure initialized on the basis of prior information that, for instance, may correspond to the bone mean speed of sound for equivalent age and health status of the patient.

Then, the expression of the corrected Radon transform is:

$$\left[R_{cc} f \right](s, \varphi) = \int f(\underline{x}) \frac{\delta(s + c_0 \tau(\underline{x}) - |r - \underline{x}| - |\underline{x} - \underline{e}|)}{16 \pi^2 |r - \underline{x}| |\underline{x} - \underline{e}|} d\underline{x} \quad (25)$$

The corrected inverse elliptical Radon transform is built from the corrected elliptical backprojection operator:

$$\left[R_{cc} \right]^{-1} = B_c \circ F^{-1} \circ Abs \circ F \text{ where } B_c h(\underline{x}) = B \left[h(\underline{n}_\varphi \bullet \underline{x} + c_0 \tau(\underline{x}), \varphi) \right] \quad (26)$$

The imaging procedure: Contrast imaging, for instance, assessing "cortical thickness" in bone imaging, consists mainly in assimilating the background comprising two areas: the reference surround medium (generally water) and the homogeneous solid part (cortical bone). The default sought for corresponds to a perturbation in that cortical area that creates a cavity in it.

A first practical approach in operating with reflection measurements (reflectivity imaging) consists in using low frequency (≤ 1 MHz) activation in order to take advantage of the large penetration depth. In that case, the Born Approximation (BA) is still met since firstly the wavelength is large compared with the size of the heterogeneity and secondly, the fluctuations of the mechanical parameters inside the cavity are small. The "constant background" inversion procedure can be based on an Elliptical Back-Projection algorithm (20) complemented with specific signal processing refinements (deconvolution). There, despite the artifacts and biases affecting the assessment of the shell thickness, good quality (contrast and resolution) images may be obtained [15].

In a second approach, one can adopt the Born Approximation (BA) with "a variable background" which consists in considering the hard medium as homogeneous while its geometry and the mean speed of sound are unknown. This requires an iterative inversion methodology, which is generally used whenever quantitative information (speed of sound distribution) is sought for. Indeed, in this case, finding solutions involves either using non-linear schemes or performing extensive studies that expand the boundaries of the use of the Born series. The so-called Distorted Born Iterative (DBI)

method is a mixed approach that implicitly specifies both the field inside the object and the Green function. Then starting from (8), one can write the expression of the measured scattered field:

$$p_{dm}(r, \underline{e}, t) = G_b \widehat{*} S^* *_i p_b(r, \underline{e}, t) \quad (27)$$

G_b is the Green function of the “variable background” (the hard medium is considered as homogeneous, but its geometry and its mean speed of sound are unknown), and p_b is the associated field so that the total measured field is:

$$p_{dm}(r, \underline{e}, t) = p_i(r, \underline{e}, t) + G_b \widehat{*} S^* *_i p_b(r, \underline{e}, t). \quad (28)$$

The three unknowns in (28) are the Green function, the field inside the object and contrast function S^* . These variables are assessed using the following iterative algorithm:

$$\left\{ \begin{array}{l} S_{est}^{*n} [R_{ec}^n]^{-1} (p_{dm}) \\ S_{est}^{*n}(\underline{x}) = (c^n(\underline{x}), \xi^n(\underline{x})) \\ \tau^{n-1}(r, \underline{e}, \underline{x}) = \frac{1}{c_0} \int_{\underline{e}\underline{x} + r} \frac{c^{n-1}(\underline{x}) - c_0}{c_0} d\underline{x}, \quad \tau^0(\underline{x}) = 0 \\ [R_{ec}^n]^{-1} = B_c^{n-1} \circ F^{-1} \circ Abs \circ F \\ p_b^{n-1}(r, \underline{e}, t) = p_i(r, \underline{e}, t + \tau_e^{n-1}(r)) \\ G_b^{n-1}(r, \underline{e}, t) = G(r, \underline{e}, t + \tau_e^{n-1}(r)) \end{array} \right. \quad (29)$$

Nota 1: When the measurements are made in transmission, $S_{est}^{*n}(\underline{x})$ gives access to the sound speed distribution, $c^n(\underline{x})$. In reflection, a band pass filtered version of the log-impedance, $\xi^n(\underline{x})$, may be obtained.

Nota 2: The last two relations are implicitly obtained but not evaluated.

To begin with, we proposed the Compound Quantitative Ultrasonic Tomography (CQUT), where refraction is taken into account in order to impose (almost) straight ray propagation inside the shell. From *a priori* knowledge of the geometrical properties and of the average acoustical parameters (speed of sound), the incident and refracted angles are estimated using the Snell-Descartes laws. Then, a compensation procedure is introduced into the scanning (e.g., by using a beam former) in order to obtain parallel paths within the “homogeneous” contrasted medium [4]. In an iterative experimental sequence, reflection and transmission measurements enable one to delineate the boundaries of the shell (the cortical region) and to assess the values of the speed of sound along the wave paths. The estimated speed of sound map obtained at iteration n is used as the geometrical and parametrical *a priori* information for step $n+1$. The stop criterion corresponds to a difference between the mean velocities calculated for two successive iterations lower than 5 m/s.

A second non-linear inversion method (i.e. the Distorted Born Diffraction Tomography (DBDT), which is also based on the DBI method) was therefore investigated. The medium is modeled without any *a priori* knowledge by performing a simple geometrical discretization of the object. The algorithm involves successive linearizations of the integral representation. The initial guess in the iterative process is provided by the first-order Born approximation. If the solution is known with the order $(n-1)$, the n -order solution will satisfy [16]. At each iteration, the algorithm solves a forward diffraction problem in order to calculate the appropriate inhomogeneous Green function G_b^{n-1} and the internal pressure

field p_b^{n-1} . Contrary to what occurs with the CQUT, the DBDT requires only a single series of experimental diffraction data. However, it is computational time consuming because it involves inversion of huge, full and complex matrix. The matrix inversion procedure is the key point with this method. Generally non-square ill-conditioned matrixes have to be inverted. A mean-square solution can be calculated using a conjugated-gradient method associated with a regularization procedure [17, 18]. To make use of the broadband frequency content of the impulse signal used, the idea is to begin at the low frequencies, which carry overall information, and to gradually inject the high frequencies to simultaneously improve both the qualitative aspects (the resolution) and the quantitative aspects (the parameterization).

3. EXPERIMENTAL IMAGING

The feasibility of UCT methods was tested on data obtained using ultrasonic scanners (Figure 2), which permits diffraction, reflection and/or transmission measurements (except for DBDT– see §1.1.6). The UCT reconstruction algorithm and the signal processing modules are implemented on a standard personal computer.

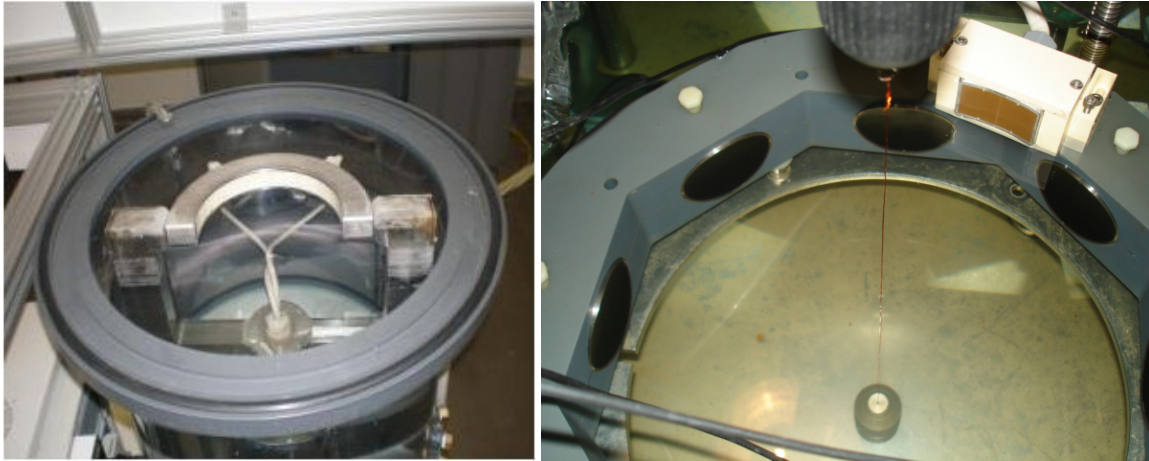


Figure 2: (Left) Soft tissues imaging: a semi-circular multi-channel 3 MHz-antenna, using 1024 piezo-composite elements. The front-end electronics incorporate 32 independent parallel transmit/receive channels and a 32-to-1024 multiplexer unit for fast acquisition of signals (7 sec.) [13] (Right) Hard tissues imaging: a 2D-ring antenna using 8 piezo-composite 1 MHz-transducers, and a 3 MHz-array using 128 piezo-composite elements. The front-end electronics incorporate 8 independent parallel transmit/receive channels and a 8-to-128 multiplexer unit for fast acquisition of signals (1 sec.)

1.1.4. Soft-tissue experimental imaging (pure fluid approximation).

The breast training phantom CIRS Model 052A mimics the ultrasonic and anatomic characteristics of tissues found on an average patient in a supine position. The flesh-like phantom made of Zerdine® contains cystic and solid masses which appear respectively dark and bright on the ultrasound and tomographic images. In Figure 3, the echographic view shows four inclusions while the tomographic reconstruction (Figure 4) reveals eight inclusions (five cysts, three masses). These differences are due, on the one hand, to a sharper directivity (thinner cross-section) of the conventional probe, which operates at a central frequency more than twice that used by the tomographic array. On the other hand, the scanner performs an entire 2D circular scan ($\text{Ø} = 30 \text{ cm}$, 720 reflection measurements) around the breast phantom whereas a unique position of the probe (one incident direction) is considered with the echographic system.



Figure 3: Echographic view (Mindray, 7.5 MHz) of breast training phantom CIRS Model 052A

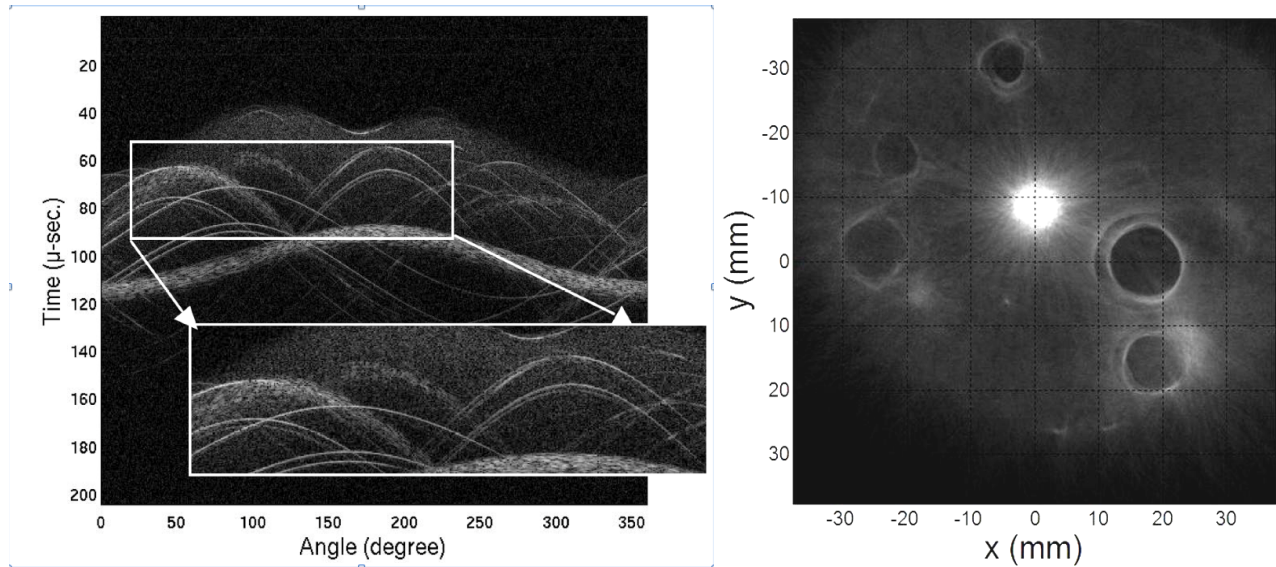


Figure 4: (Left) Sinogram (3MHz) of the phantom (Right) Tomographic reconstruction (3 MHz) of the same region of the phantom as in Figure 3.

Comments: With sonographic semiology, cysts are generally the easiest ones to diagnose reliably since they are round or oval anechoic lesions with smooth wall contours and dorsal echo enhancement. On the contrary, on echographic view, the dense solid mass generates bright echoes at the sound-entrance border and a shadow behind the lesion. These two artifacts (echo enhancement and shadowing) are not reproduced with the tomographic approach (Figure 4). Besides, the Zerdine matrix is depicted with important speckle noise on the echographic image. This noise is strongly reduced on the tomographic representation since the point-spread function of the scanner is recognized as being more isotropic and spatially concentrated than that of the echographic device. Furthermore, circular rings are visible round certain cysts (e.g. the larger one); the corresponding echoes are observed on the sinogram (Figure 4 - left). These rings are slightly perceptible in the conventional ultrasound image depicted in Figure 5 – left, where a zoom is performed on the largest cyst (equatorial plane). These views confirm that, within the matrix, an interface exists which delineates a Zerdine layer around the cystic inclusions. Considering the tomographic approach (Figure 5 - right), this “weak” interface is revealed distinctly by the coherent summation performed over a large aperture of the interrogating wavefront. On the contrary, using conventional ultrasounds, the continuity of the (Zerdine) material induces low level backscattering of the focused transmit waves.

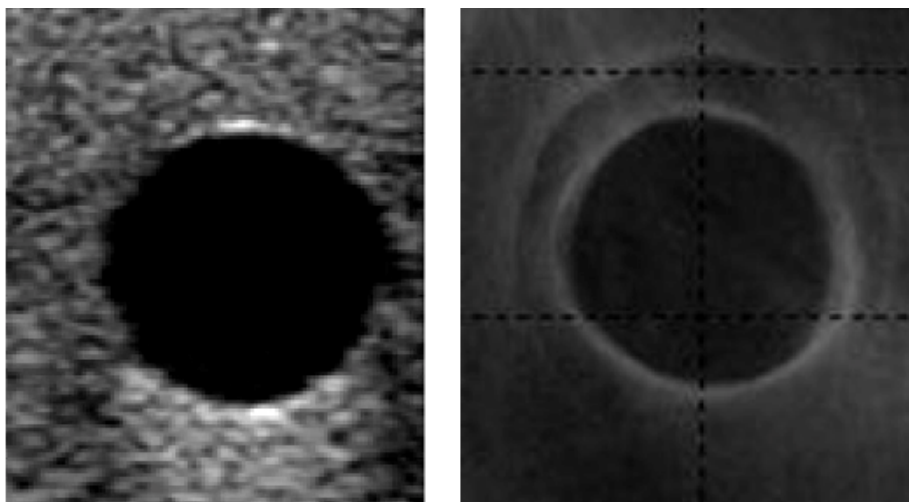


Figure 5: Comparison of conventional (left) and UCT (right) image of the cyst phantom (zoom of the Figure 4 - right).

However, one reservation must be made concerning tomographic representations: the contour of the dense mass appears slightly speculated. This is because of its strong echogenicity, which associates high values with the elliptical back-projections crossing the lesion domain. This effect may be reduced by using a large aperture phased array in reflection that attenuates the reconstruction noise, as in [9, 13].

1.1.5. Bone experimental qualitative imaging (fluid-like approximation).

3-D UCTs (Figure 6) of child's fibula were obtained from diffracted measurements. The nominal frequency of the transducers was 1 MHz. The resolution and the size of the image were 0.75 x 0.75 mm and 512 x 512 pixels, respectively. The diffracted sinograms included 2048 projections, each including 8192 samples, involving 32 angular transmitter positions combined with 64 angular receiver positions covering an angle of 360°. The sampling frequency used was 40 MHz. A signal-processing tool [19] was used to determine cortical thickness. This tool was based on a segmentation of the final image and a size correction of the inner boundaries, using a priori information on physical parameters (in this case, mean compressional wave velocity in bone = $3500 \pm 100 \text{ m.s}^{-1}$, bone mass density = 1700 kg.m^{-3}). The 3-D UCT images were obtained by superimposing sequential 2-D UCT images (20 cross-sections). The step between two cross-sections was 1 mm. The interpolation scheme used for a given 3-D image was the shape-based method (Matlab®, MathWorks™).

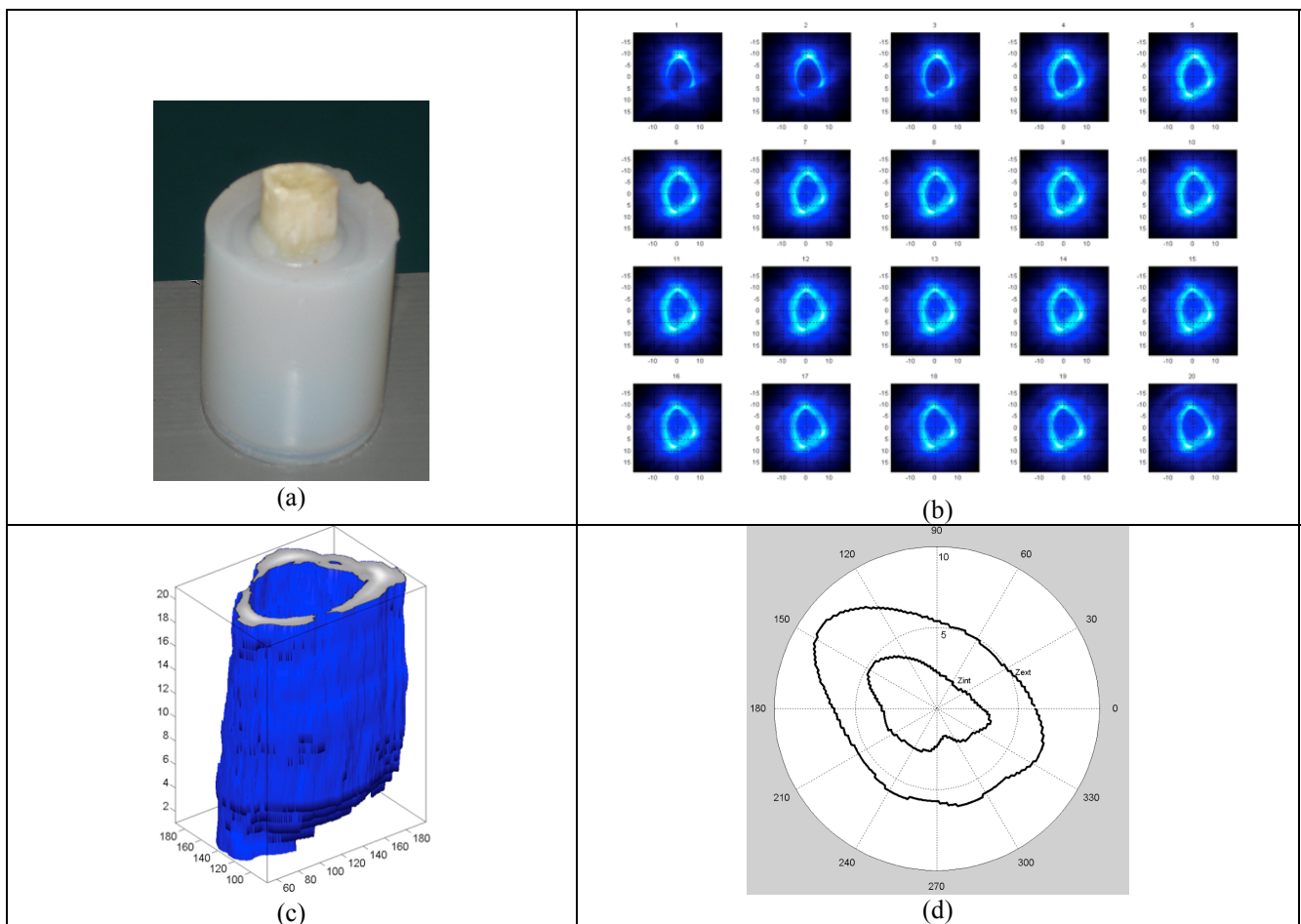


Figure 6: Cortical thickness of a 12-year old child's fibula (a) sample embedded in an agar-gel shell (b) Twenty sequential cross-sections were performed in this case with a 1-mm step (c) 3-D tomogram (300 x 300 pixels) (d) the mean dimensions (after processing) of the bone sample were 7 ± 2 mm on the outside and 3 ± 2 mm in the inner cavity.

Figure 7 shows 2-D UCT of artificial paired bones (fibula and femur). The both bones show up particularly clearly. But, the zone between the thighbone and the fibula is not clearly imaged and it is impossible to measure the distance between

the both bones. The copper rod, placed in-between, isn't visible too. This was mainly due to the multiple diffusion, refraction and others phenomenon, occurring.

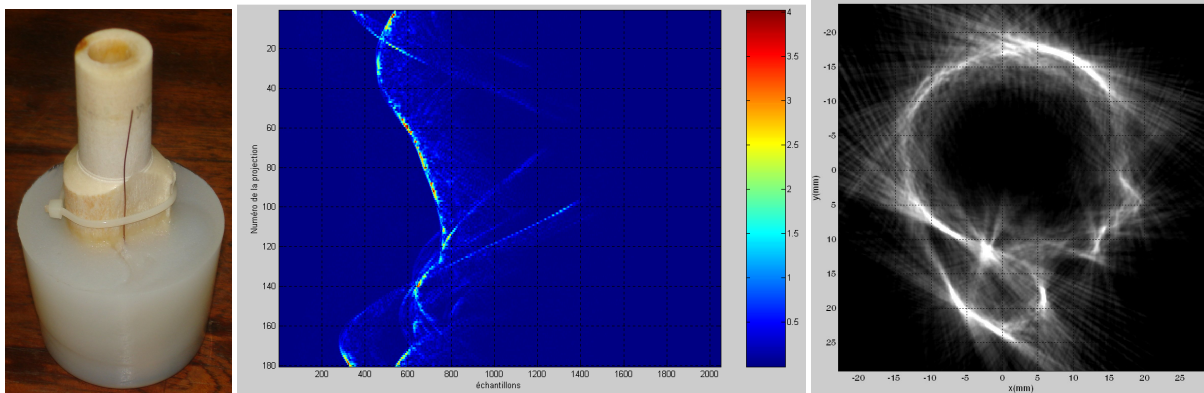


Figure 7: 2-D UCT of adjacent fibula and femur bones, 300 x 300 pixels

However, these results obtained with human specimens show that it is possible to characterize the size and shape of bones using Ultrasonic Computer Tomography. Focusing on well-contrasted images obtained using UCT show that this method provides efficient means of assessing the cortical thickness, which is known to be an important indicator of bone strength.

1.1.6. "Bone" experimental quantitative imaging (fluid-like approximation).

The aim here is to obtain information about the shape, dimensions and sound speed profile of the studied object. Classical diffraction tomographic methods based on the first-order Born approximation give good results for weakly scattering targets but fail when it comes to give a quantitative information, such as the sound speed profile, for high impedance contrast targets such as bones. In this case, the first-order Born approximation is no longer valid. We propose to use the DBDT to overcome this difficulty. This is an iterative process that successively solves a linearized inverse problem involving the minimization of the discrepancy between the measured and computed scattered fields [6, 17]. The stability of the inversion process is enhanced by means of Tikhonov regularization.

An experimental study was performed with a non-circular homogeneous isotropic shell made of artificial resin (NEUKADUR ProtoCast 113TM). The mass density of the resin was 1150 kg.m^{-3} , and the mean velocity of the compressional wave was $2400 + 50 \text{ m/s}$. The surrounding fluid-like medium (and the hollow area) was water at a temperature of 18° (mass density: 1000 kg.m^{-3} , sound speed: 1480 m/s). The transmitter and the receiver were placed at 17.5 cm to the center of the bench. Ultrasounds were generated using a pulser transmitter/receiver device (Panametrics HP 5055PR) and wide-band Panametrics transducers. We used successively two pairs of transducers with a nominal frequency of 0.250 MHz and 1 MHz , respectively. The usable bandwidth range from approximately 135 kHz to 375 kHz and from 500 kHz to 1.5 MHz . The object was placed in the center of the measuring system. The sector scanned was 360 degrees around the target with both transducers with an angular increment of 10 degrees (36×36 signals for each paired transducer).

Iterations were performed by gradually increasing the working frequency with 3 frequencies chosen in the transducers bandwidth: 150 kHz , 350 kHz and 1 MHz . For iterations at 150 kHz , the first-order Born approximation solution is used as an initial guess. At other frequencies, the initial guess was the final result of the iteration process performed at the previous frequency (for example, the result of the inversions performed at 150 kHz was used as the initial guess for the inversions performed at 350 kHz , etc).

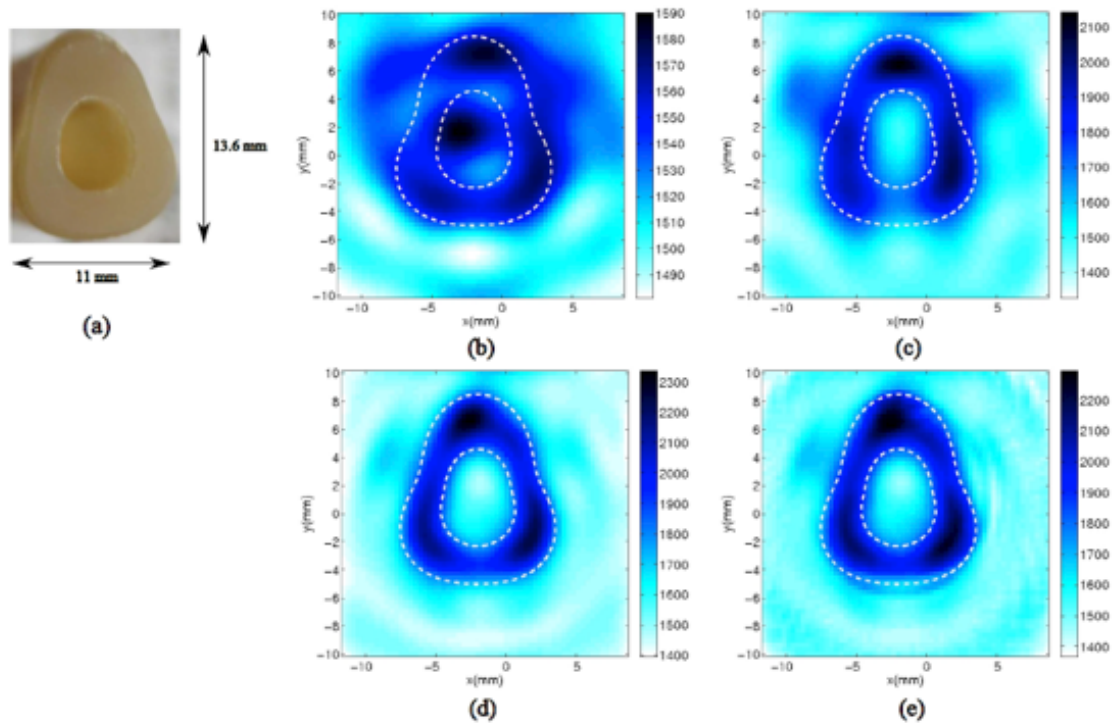


Figure 8: (a) NEUKADUR ProtoCast 113TM resin target. Results of DBDT: (b) first-order Born solution at 150 kHz, (c) after iterations at 150 kHz, (d) after iterations at 350 kHz and (e) after iterations at 1 MHz.

Figure 8 show the first-order Born solution and three sequential iterations of the DBDT. It can be seen that the resolution and the quality of the contrast is gradually improved. The final result of the iteration process was satisfactory. The geometry was fairly accurate (position and dimensions reconstructed with mean relative error of the order of 5%) and the velocity was estimated with a relative error of about 10 %.

4. CONCLUSION

Ultrasound Computer Tomography (UCT) appears as an alternative imaging tool able to reveal the internal structure of soft tissues (mammography), to delineate the shape of bones (cortical thickness) and even to provide the possibility of parametric estimation (the sound speed map).

The theoretical framework corresponds to the analytical formulation (Green function) of the forward problem considering point-like transmitters and receivers. Thus the shape of the transmitted wave (the incident field) is spherical, as are also assumed to be the secondary sources induced by the elementary scatterers of the investigated media.

As regards soft tissue imaging, the derivation of the near-field forward problem has led us to define new elliptical Fourier transforms and associated elliptical Radon transforms. Using these two transform pairs (direct and inverse transforms) the contributions in the scattered field of impedance and of sound speed respectively can be separated. This opens the way to single parametric reconstruction (imaging) i.e. to assessing the distribution of the acoustical parameters using optimized numerical procedures (Fast Fourier Transforms).

For highly heterogeneous media having greater acoustical impedances and speed of sound than those of the surrounding medium, additional consideration of a “variable (homogeneous) background” is necessary if one seeks parametric imaging. Here, the strong non-linearities in the parametric distributions have been dealt with using an iterative inversion procedure.

The examples dealt with in this paper were industrial breast phantoms and real thighbones. In comparison with conventional ultrasounds, UCT methods applied to soft tissues offer reduced speckle noise, artifact-free representation, and enhanced quality (point resolution and contrast) imagery. However, in the vicinity of hard lesions, the presence of strong scatterers may induce some reconstruction noise that could affect the image interpretation (spiculated artifact).

Theoretical considerations have demonstrated that large aperture measurements in reflection improve the robustness of the reconstruction. This approach is currently under development [13].

Applied to bone imaging, UCT methods give geometrical information of poorer quality (coarser resolution, geometrical distortions), but the reconstruction obtained is still clinically relevant, especially in the case of children's bones. Besides, the mechanical assessments provided are in direct connection with medical demand (i.e. modeling and strength status of the bone) and it is a non-ionizing modality that can be used in pediatric care. However, estimations of geometry and mechanical information must be associated in a common procedure. Ultimately, the improvement in image quality and in accuracy will be obtained only with a more refined characterization of the 3-D cortical structure. The definition of this structure will specify the "distorted" 3-D Green function, i.e. the conditions of propagation in that cortical structure.

ACKNOWLEDGMENT

The authors are grateful for medical assistance to Drs D. Amy, radiologist, Aix en Provence, Dr P. Petit and Dr J.-L. Jouve at Public Assistance Hospitals and the "Timone" Children's Hospital in Marseille. Our thanks also go to Eric Debieu, Stephan Devic, and Alain Busso for their technical assistance. This study was based on research supported by the National Center for Scientific Research (CNRS), the *Canceropôle PACA*, the *Provence-Alpes-Côtes d'Azur* Council, and the French National Research Agency (ANR).

REFERENCES

- 1 Ouedraogo E., Lasaygues P., Lefebvre J.P., Gindre M., Talmant M., Laugier P. "Multi-step compensation technique for ultrasound tomography of bone," *Acoustical Imaging* 26, 153-160, (2001).
- 2 Teng X., "Application of ultrasonic tomography in industrial materials", The John Hopkins University (1993).
- 3 Ouedraogo E., Lasaygues P., Lefebvre J.P., Gindre M., Talmant M., and Laugier P. "Contrast and velocity ultrasonic tomography of long bones," *Ultrasonic Imaging* 24, 135-146 (2002).
- 4 Lasaygues P., Ouedraogo E., Lefebvre J.-P., Gindre M., Talmant M. and Laugier P., "Progress toward in vitro quantitative imaging of human femur using Compound Quantitative Ultrasonic Tomography," *Phys. Med. Biol.*, 5(11), 2633-2649 (2005).
- 5 Lu C., Lin J., Chew W.C., and Otto G. "Image reconstruction with acoustic measurement using distorted Born iteration method," *Ultrasonic Imaging*, 18(2), 140-156 (1996).
- 6 Lasaygues P., Guillermin R. and Lefebvre J.-P. *Ultrasonic Computed Tomography*," Bone Quantitative Ultrasound, P. Laugier & G. Haiat Eds, Springer, 441-459 (2010).
- 7 Greenleaf J. F., "Introduction to Computer Ultrasound Tomography," *Computed Aided Tomography and Ultrasonics in Medicine*, North-Holland, 125-136, (1970).
- 8 Andre M.P., Martin P.J., Otto G.P., Olson L.K. and T.K. Barrett, "A new consideration of diffraction computed tomography for breast imaging: Studies in phantoms and patients," *Acoustical Imaging*, J.P. Jones Ed., 379-390, (1995).
- 9 Mensah S. and Lefebvre J.-P., "Enhanced Compressibility Tomography," *IEEE Trans. Ultrason., Ferroelec., Freq. Contr.*, vol. 44(66), 1245-1252, (1997).
- 10 Franceschini E., Mensah S., Le Marrec L. and Lasaygues P., "An optimization method for quantitative impedance tomography," *IEEE Trans. Ultrason., Ferroelec., Freq. Contr.*- Special Issue on High Resolution Ultrasonic Imaging in Industrial, Material and Biomaterial Applications, 54(8), 1578 – 1588, (2007).
- 11 André M.P., Janée H.S., Martin P.J., Otto G.P., Spivey B.A. and Palmer D.A., "High-speed data acquisition in diffraction tomography system employing large-scale toroidal arrays," *International Journal of Imaging System and Technology*, 8(1), 137-147, (1998).
- 12 Waag R.C. and Fedewa R.J., "A ring transducer system for medical ultrasound research," *IEEE Trans. Ultrason., Ferroelec., Freq. Contr.*, 53(10), 1707-18, (2006).
- 13 Rouyer J., Lasaygues P., Mensah S., Franceschini E. and Lefebvre J.P., "Conformal Ultrasound Imaging System for Anatomical Breast Inspection," *IEEE Trans. On Ultrasonics, Ferroelectric and Frequency Control*, Special Issue on "Novel Embedded Systems for Ultrasonic Imaging and Signal Processing", (to appear 2012).
- 14 Mensah S. and Franceschini E., "Near field tomography," *JASA*, 121(3), 1423-1433, (2007).
- 15 Lasaygues P. and Lefebvre J.-P., "Cancellous and cortical bone imaging by reflected tomography," *Ultrasonic Imaging*, 23(1), 55-68, (2001).

-
- 16 Haddadin O. S., "Ultrasound inverse scattering for tomographic imaging self-focusing array", University of Michigan, (1998).
- 17 Lasaygues P., Guillermin R. and Lefebvre J.-P., "Distorted Born diffraction tomography applied to inverting ultrasonic field scattered by noncircular infinite elastic tube," *Ultrasonic Imaging*, 28(4), 211-229 (2006).
- 18 Guillermin R., Lasaygues P., Rabau G. and Lefebvre J.-P., "Quantitative non-linear ultrasonic imaging high-impedance contrast targets - An experimental investigation," submitted *Inverse problem*, (2011).
- 19 Lasaygues P., "Assessing the cortical thickness of long bone shafts in children, using two-dimensional ultrasonic diffraction tomography," *Ultrasound in Med. & Biol.*, 12(8), 1215-1227 (2006).